eLIFE
elifesciences.org

Figures and figure supplements

Genomic mosaicism with increased amyloid precursor protein (*APP*) gene copy number in single neurons from sporadic Alzheimer's disease brains

Diane M Bushman, et al.

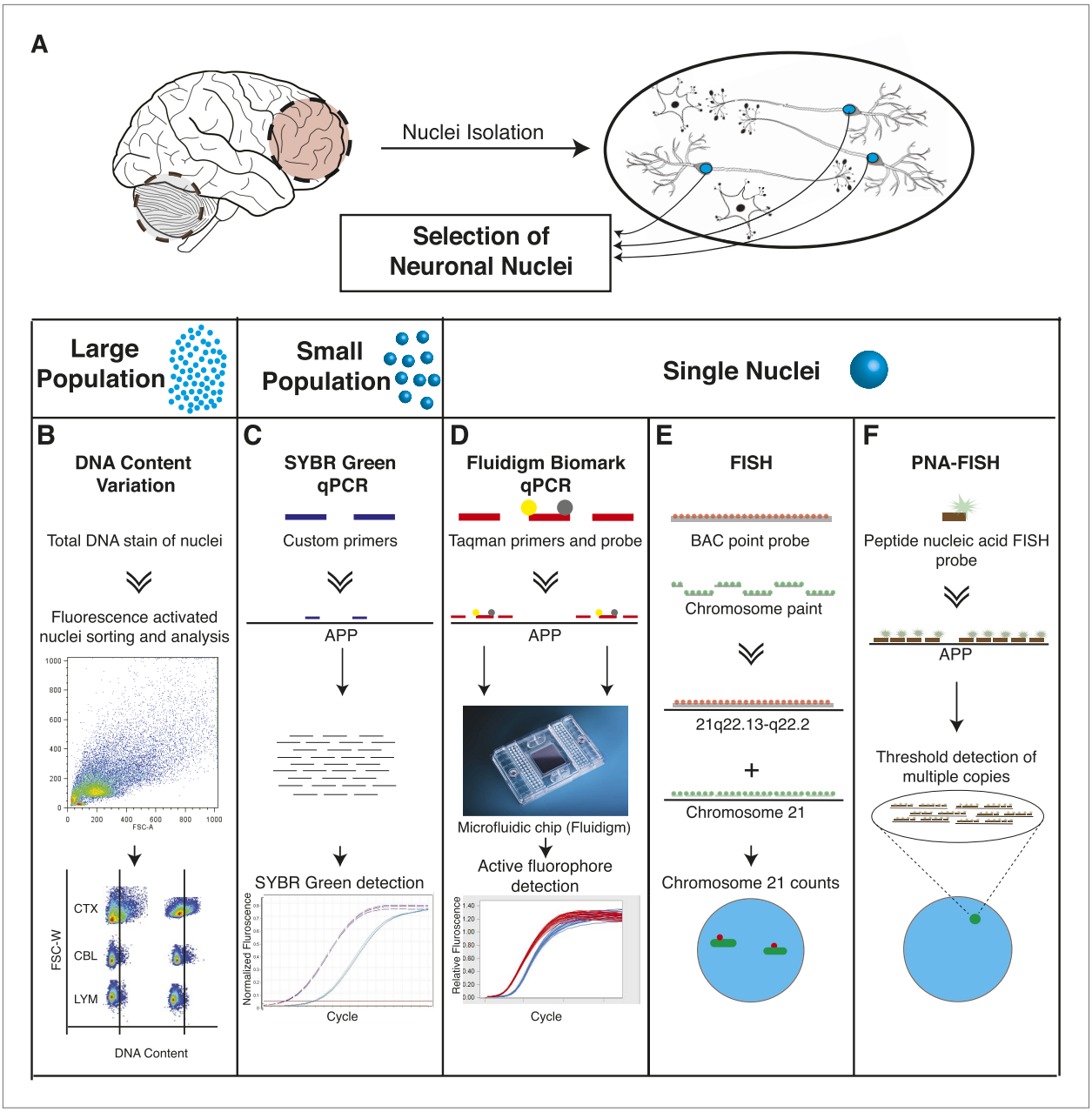

Figure 1. Methodologies used in assessing genomically mosaic AD. (**A**) Neuronal nuclei were isolated from the prefrontal cortex and cerebellum of postmortem human brain (see 'Materials and methods' for samples used) as described (***Westra et al., 2008***). (**B**) Nuclear DNA was stained with propidium iodide (PI) and DNA content was quantified using flow cytometric analysis. (**C**) *APP* copy number variations were analyzed in small populations of nuclei (~75 genomes) using custom primers for exon 14 of *APP*. (**D**) Single-cell qPCR assessed *APP* copy number variations in individual neuronal nuclei via TaqMan probes and a modified Biomark integrated fluidic chip system (Fluidigm Corporation, South San Francisco). (**E**) FISH paints against the whole q arm of chromosome 21 and a point probe against a region on the q arm of 21 (21q22.13-q22.2) were used to double-label and call aneusomies in AD samples. (**F**) Peptide nucleic acid (PNA) FISH was combined with super resolution microscopy for threshold detection of *APP* copy number above ~2 occurring at a single locus.

DOI: 10.7554/eLife.05116.003

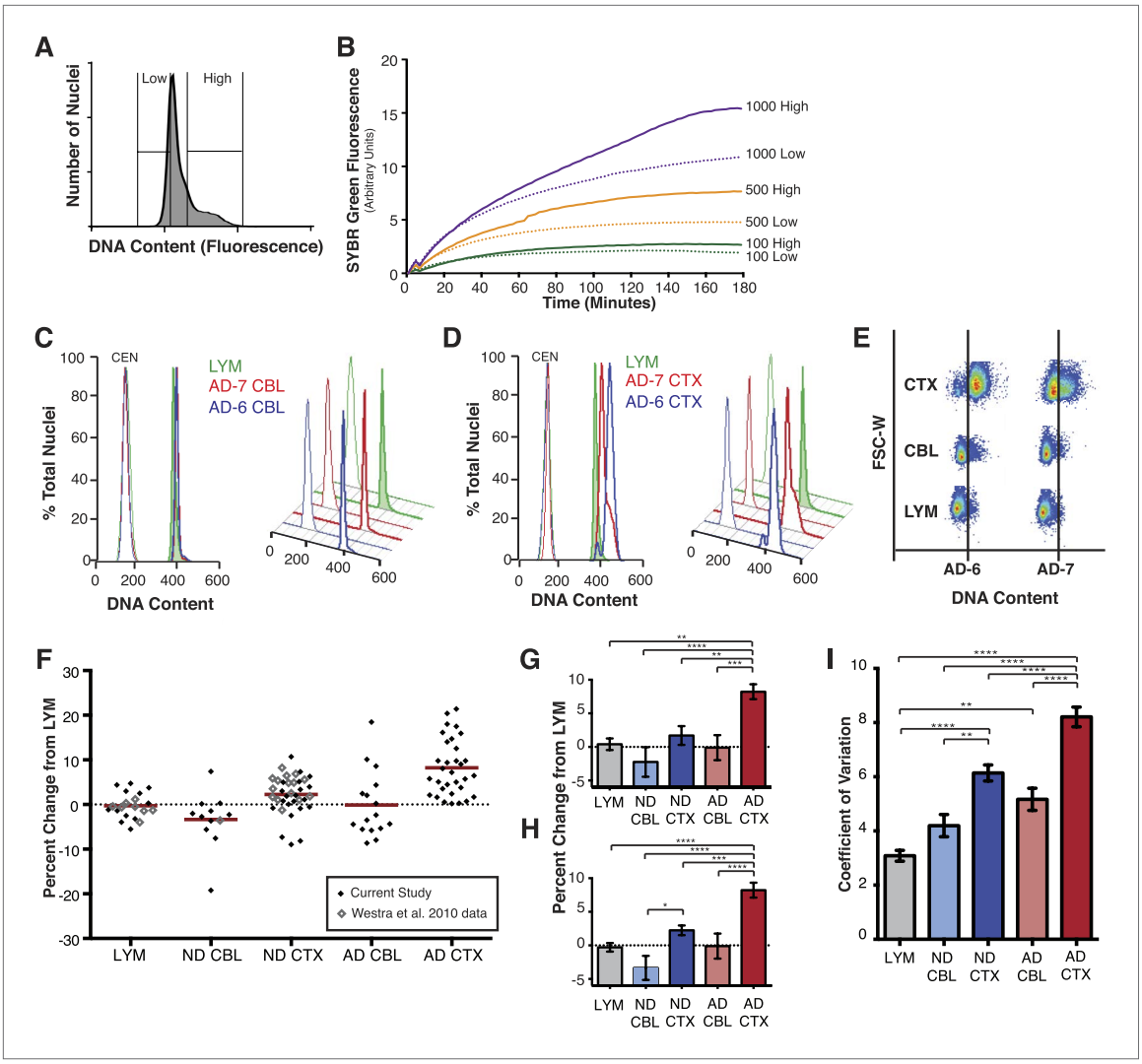

Figure 2. AD cortical nuclei show increased DNA content variation (DCV) by flow cytometry. (**A**) Histogram displaying gating parameters used in sorting 'high' and 'low' DNA content populations for validation of DNA content. (**B**) Validation of DNA content analyses using semi-quantitative MDA whole-genome amplification (WGA) on 'high' and 'low' DNA content populations of 1000, 500, and 100 nuclei. (**C** and **D**) Representative DNA content histograms for lymphocytes (LYM), AD cerebellum (CBL), and AD prefrontal cortex (CTX). Each colored histogram represents a separate sample in each set; CTX and CBL samples are from paired brains. Chicken erythrocyte nuclei (CEN) were used as internal calibration controls. (**E**) Representative orthogonal view of DNA content vs forward scatter width (FSC-W). For each brain sample, the area to the right of the vertical line indicates a DNA content increase of the population of nuclei. AD-6 CTX is a representative right-hand peak shift and AD-7 is a representative right-hand shoulder (see ***Figure 3A*** for more examples). (**F**) DNA content changes for all human LYM, ND, and AD brain samples examined (AD CTX N = 32, AD CBL N = 16, LYM N = 15 [20 meta analysis], ND CTX = 21 [36 meta analysis], ND CBL = 11 [12 meta analysis]). Red bars denote average for each group relative to lymphocytes. Averages are as follows (including metadata from ***Westra et al. (2010)***): AD CTX 8.219%; AD CBL −0.1104%; LYM −0.2915%; ND CTX 2.239%; ND CBL −3.358%. (**G**) DNA content changes of the current study (AVOVA $p < 0.0001$). (**H**) DNA content changes of the current study combined with metadata from ***Westra et al. (2010)*** (ANOVA $p < 0.0001$). (**I**) Comparison of mean coefficient of variation (CV statistic from FlowJo of the population, included metadata from ***Westra et al., 2010***) demonstrates that there is an average increase in the variation of AD samples (ANOVA $p < 0.0001$). *p = 0.05, **p = 0.01, ***p = 0.001, ****p < 0.0001, See ***Figure 2—source data 1*** for exact p values. See ***Figure 2—figure supplement 1*** for age, PMI and Braak score correlations. See ***Figure 2—figure supplement 2*** for control of nuclear size analysis.

DOI: 10.7554/eLife.05116.004

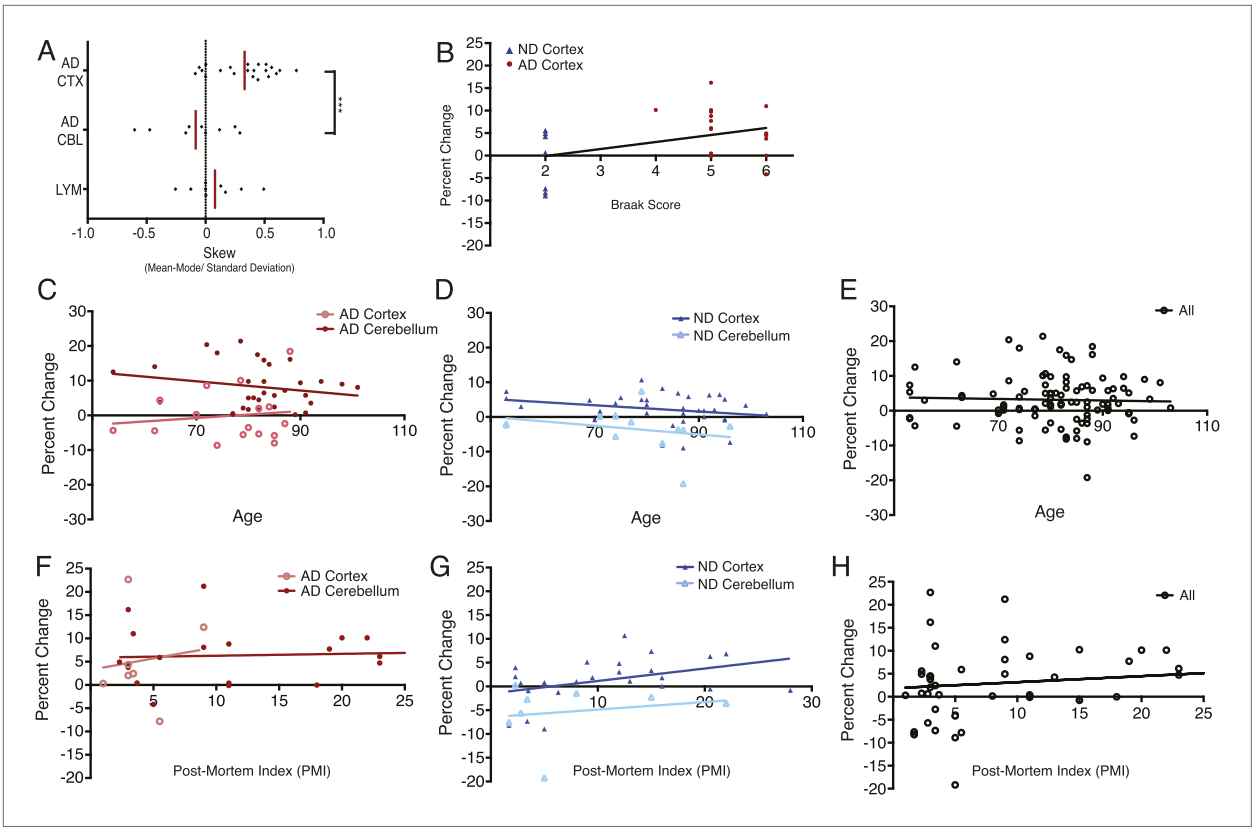

Figure 2—figure supplement 1. DNA content shows no correlation with age or post-mortem index (PMI). (**A**) Comparison of mean skew values for each sample group, skew determined as: (Mean − Mode/Standard Deviation of the diploid DNA content peak). (**B**) No correlation was observed between DNA content and Braak score. (**C**–**E**) No correlation was observed between DNA content and age across all brains analyzed. (**F**–**H**) No correlation was observed between DNA content and post-mortem index across all brains analyzed.

DOI: 10.7554/eLife.05116.006

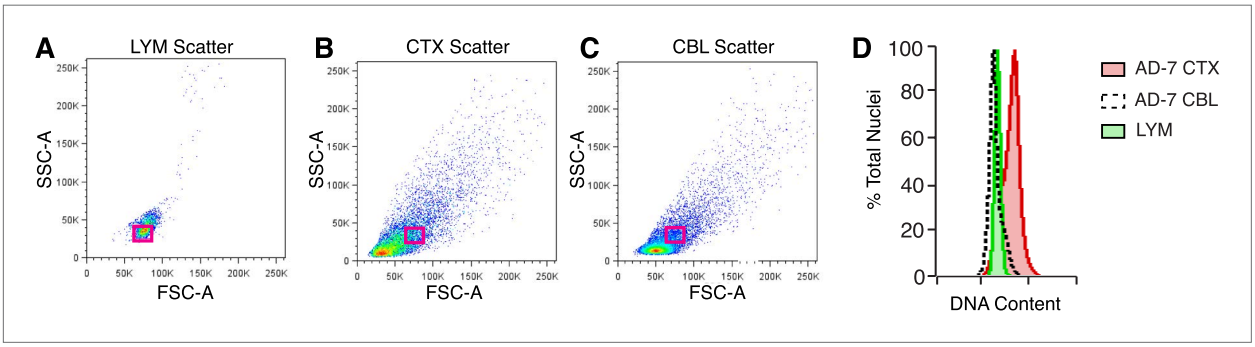

Figure 2—figure supplement 2. Analysis of nuclear size and DNA content. (**A**–**C**) Representative flow cytometry scatter plots of nuclei. (**A**) Lymphocytes (LYM), (**B**) CTX nuclei, (**C**) CBL nuclei. (**D**) Overlay of red boxes shown in (**A**–**C**), demonstrating that cortical nuclei similar in size to LYM and CBL consistently display a DNA content shift.

DOI: 10.7554/eLife.05116.007

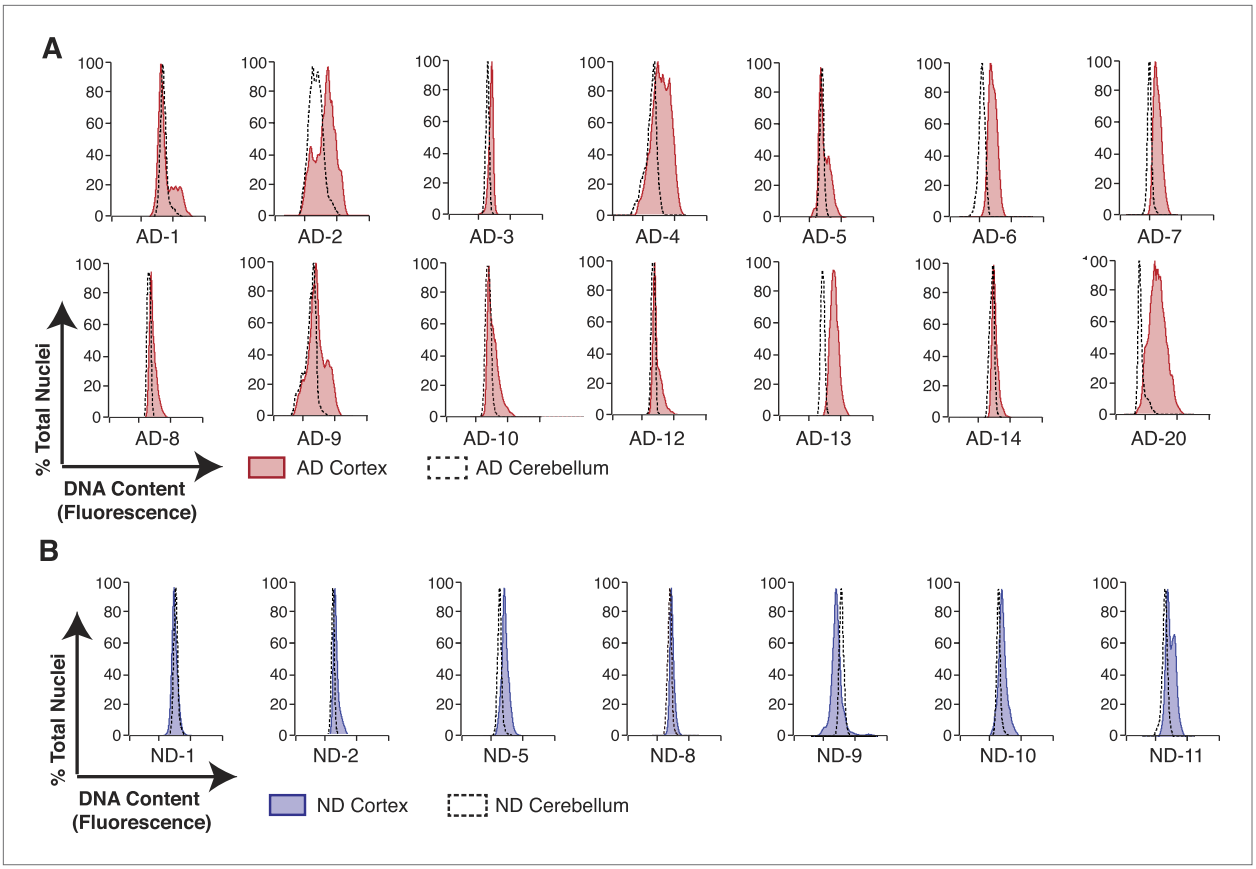

Figure 3. Pairwise DNA content analyses in AD cortical nuclei vs AD cerebellum. (**A**) Pairwise analysis of overlaid DNA content histograms (CTX = solid red, CBL = black dashed lines) in the same AD individual (each graph represents a unique AD individual). (**B**) Pairwise analysis of overlaid DNA content histograms (CTX = solid blue, CBL = black dashed lines) in the same ND individual.

DOI: 10.7554/eLife.05116.008

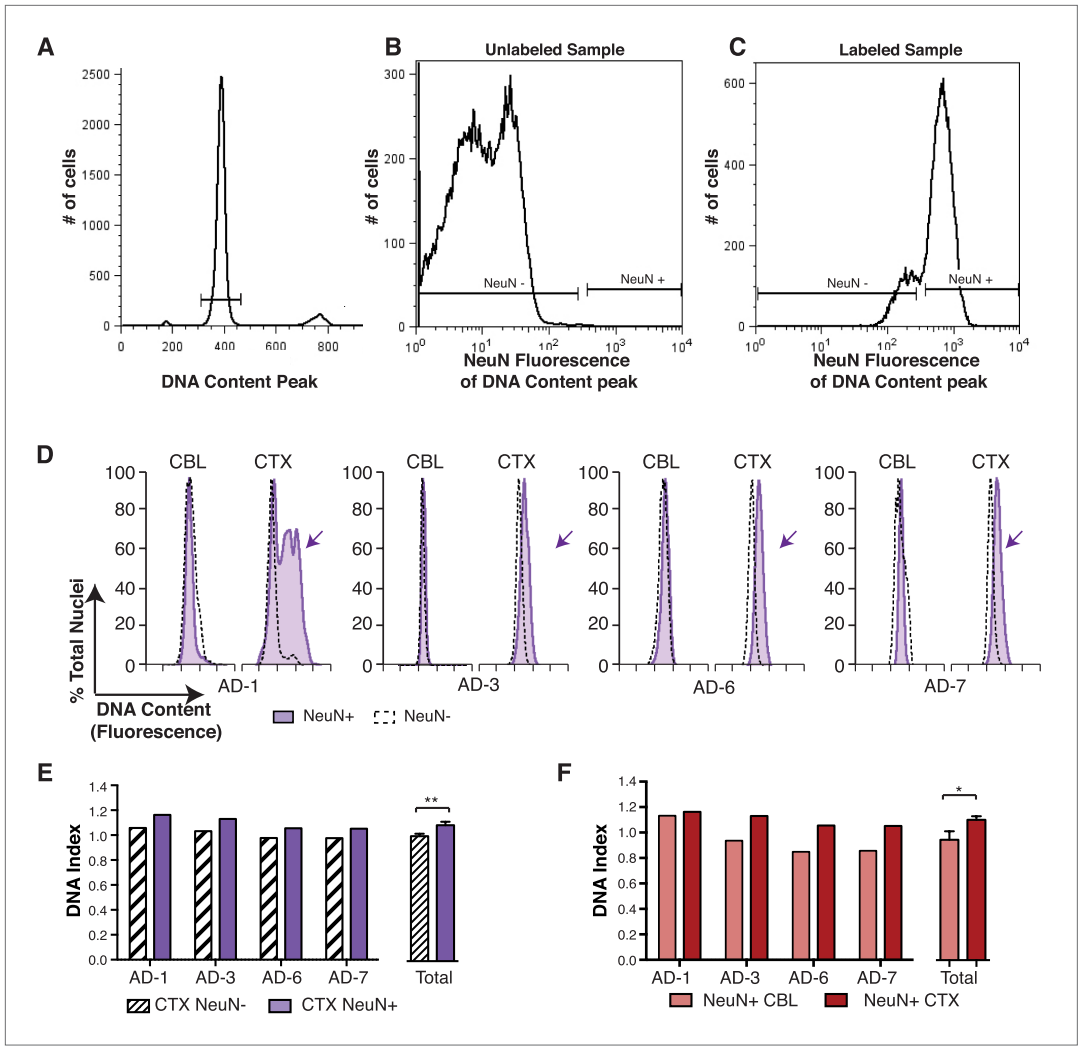

Figure 4. DNA content increases observed in AD cortical nuclei are attributable to neurons. (**A**–**C**) The gating procedure used for NeuN-positive flow cytometry analysis. (**A**) DNA content peak for identified nuclei. (**B**) A sample of unlabeled neuronal nuclei that display no NeuN-positive signal. (**C**) Selection for NeuN-positive nuclei for downstream analysis. (**D**) DNA content histograms of four AD samples displaying NeuN-positive nuclei (solid purple) vs NeuN-negative nuclei (black dashed line). NeuN-positive populations display distinct cortical histograms with prominent right-shifted peaks (arrows). (**E**) Comparison of DNA index (DI) increases from NeuN-positive nuclei (solid purple) vs NeuN-negative nuclei (black dashes) from AD CTX samples. NeuN-positive nuclei (DI = 1.10) showed an average gain of 9% over NeuN-negative nuclei (DI = 1.01), **p = 0.0011. (**F**) Comparison of DNA content in NeuN-positive nuclei from AD CTX (DI = 1.10) (red) vs AD CBL (DI = 0.94) (pink) from the same individual; CTX nuclei displayed a 15.6% gain over CBL nuclei, *p = 0.0335. Statistics are paired two-tailed *t*-test. Bars indicate ± SEM.

DOI: 10.7554/eLife.05116.009

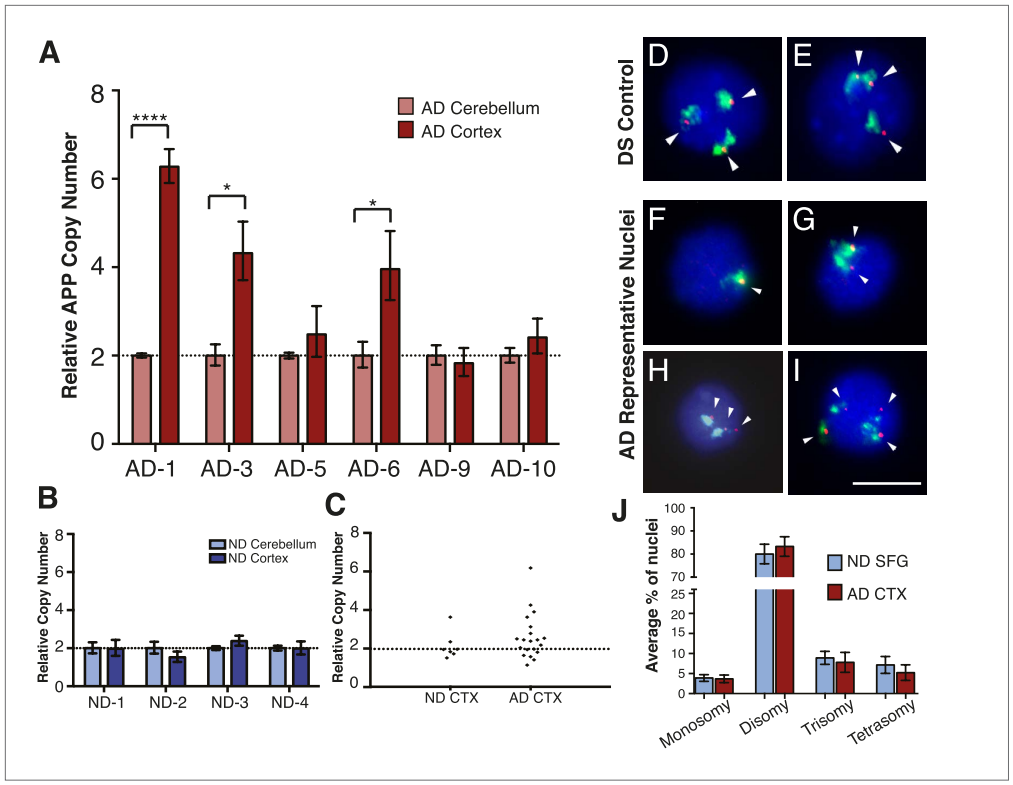

Figure 5. Mosaic amplification of the *APP* locus in small cohorts of AD cortical neurons unrelated to trisomy 21. (**A**) Comparison of relative copy number of *APP* in CBL and CTX fractions from six AD brains. *APP* locus-specific amplification was determined relative to reference gene *SEMA4A*; paired CBL nuclei were used as a calibrator sample for each brain, normalized to 2.00 for a diploid cell. Differences in ΔΔCt ± SEM of *APP* in the cortex vs cerebellum were assessed in each individual using an unpaired, two-tailed t-test (****p = 0.0001, *p = 0.0165, *p = 0.0489) (**B**) Comparison of relative copy number of *APP* in CBL and CTX fractions from 4 non-diseased brains. (**C**) Average relative copy number in non-diseased vs AD brains. Control genes and DS individuals were also examined (***Figure 5—figure supplement 1***). (**D**–**J**) FISH strategy of chromosome 21 counting through simultaneous labeling using chr 21 q arm 'whole' chromosome paint (WCP, green) and chr 21 regional FISH probe for 21q22.13-q22.2 (red) (see ***Figure 5—source data 1*** for raw counts). (**D** and **E**) The ability to detect aneuploidy was validated using interphase nuclei from a human trisomy 21 brain, where three regional spots (red, encompassing the *APP* gene) were seen, despite WCP spatial variation (see also ***Rehen et al. (2005)***). (**F**–**I**) Chromosome 21 aneusomy was examined in prefrontal cortical nuclei. Examples of chr 21 (**F**) monosomy, (**G**) disomy, (**H**) trisomy, and (**I**) tetrasomy (please note tetrasomy is not an example of aneuploidy). (**J**) Quantification of individual FISH signals showed no significant differences in monosomy, disomy, trisomy, or tetrasomy. 5 control brains and 9 AD brains were used. At least 450 nuclei were quantified per brain sample. Scale bar = 10 um. 4974 total nuclei examined.

DOI: 10.7554/eLife.05116.010

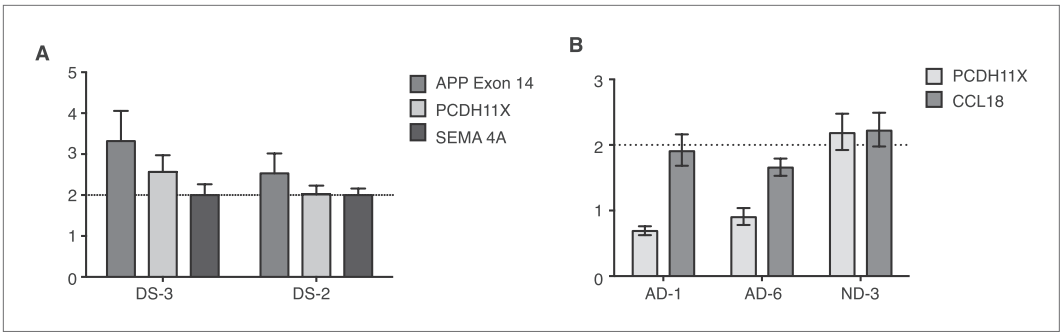

Figure 5—figure supplement 1. Controls for small population qPCR. (**A**) Reference genes validated in small population qPCR via examination of *APP* exon 14 in Down Syndrome (DS) nuclei as a positive control. (**B**) Representative males (AD-1 and AD-6) displayed reduced copy number of PCDH11X, a gene located on the X chromosome, while a representative female demonstrates two copies of PCDH11X and CCL18, a second single copy control gene.

DOI: 10.7554/eLife.05116.012

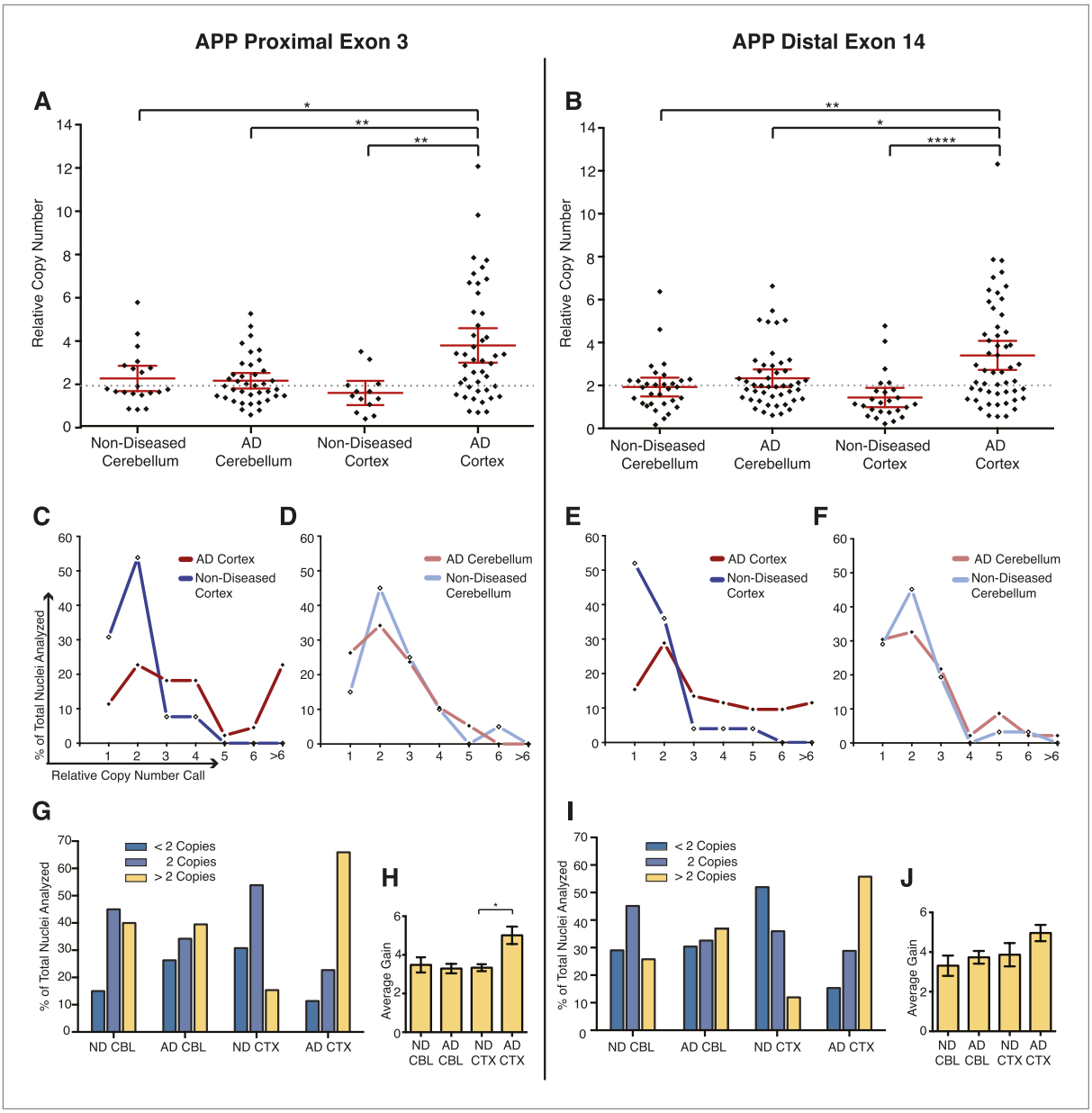

Figure 6. Mosaic *APP* locus amplification in single neurons from AD brains. (**A**) Single nuclei relative copy numbers for exon 3 of *APP* from non-diseased (ND) CBL, ND CTX, AD CBL, and AD CTX; each black diamond represents one neuron. For each group, the mean is displayed in red and bars represent 95% confidence intervals. AD CTX showed a mean *APP* copy number of 3.80; this is significantly higher than AD CBL (2.23), ND CTX (1.60), and ND CBL (2.28). *p = 0.0147, **p = 0.0015, **p < 0.0012, ANOVA p < 0.0001 (see ***Figure 6—source data 1*** for raw numbers and statistics). (**B**) Single nuclei relative copy numbers for exon 14 of *APP*, similar to (**A**). The two exons showed a high concordance (***Figure 6—figure supplement 1***) where the AD CTX showed a mean *APP* copy number of 3.40 while the AD CBL (2.34), ND CTX (1.44), and ND CBL (1.92) remained closer to 2 copies. *p = 0.0163, **p = 0.0016, ****p < 0.0001, ANOVA p < 0.0001. (**C**–**F**) Distribution of copy number calls for exon 3 (**C** and **D**) and exon 14 (**E** and **F**) binned by relative copy number. The AD CTX for both exons displayed unique distributions, with more nuclei falling into the high copy number bins. (**G** and **I**) Distribution of nuclei with copy numbers less than, equal to, and greater than two copies. (**H** and **J**) Average copy number increases in nuclei binned with greater than two copies (gold columns in **G**) (AD CTX: Exon 3 = 5.01, Exon 14 = 4.96, *p = 0.0361). All statistics represent an ANOVA with a Tukey's multiple comparison test. Bars indicate ± SEM.

DOI: 10.7554/eLife.05116.013

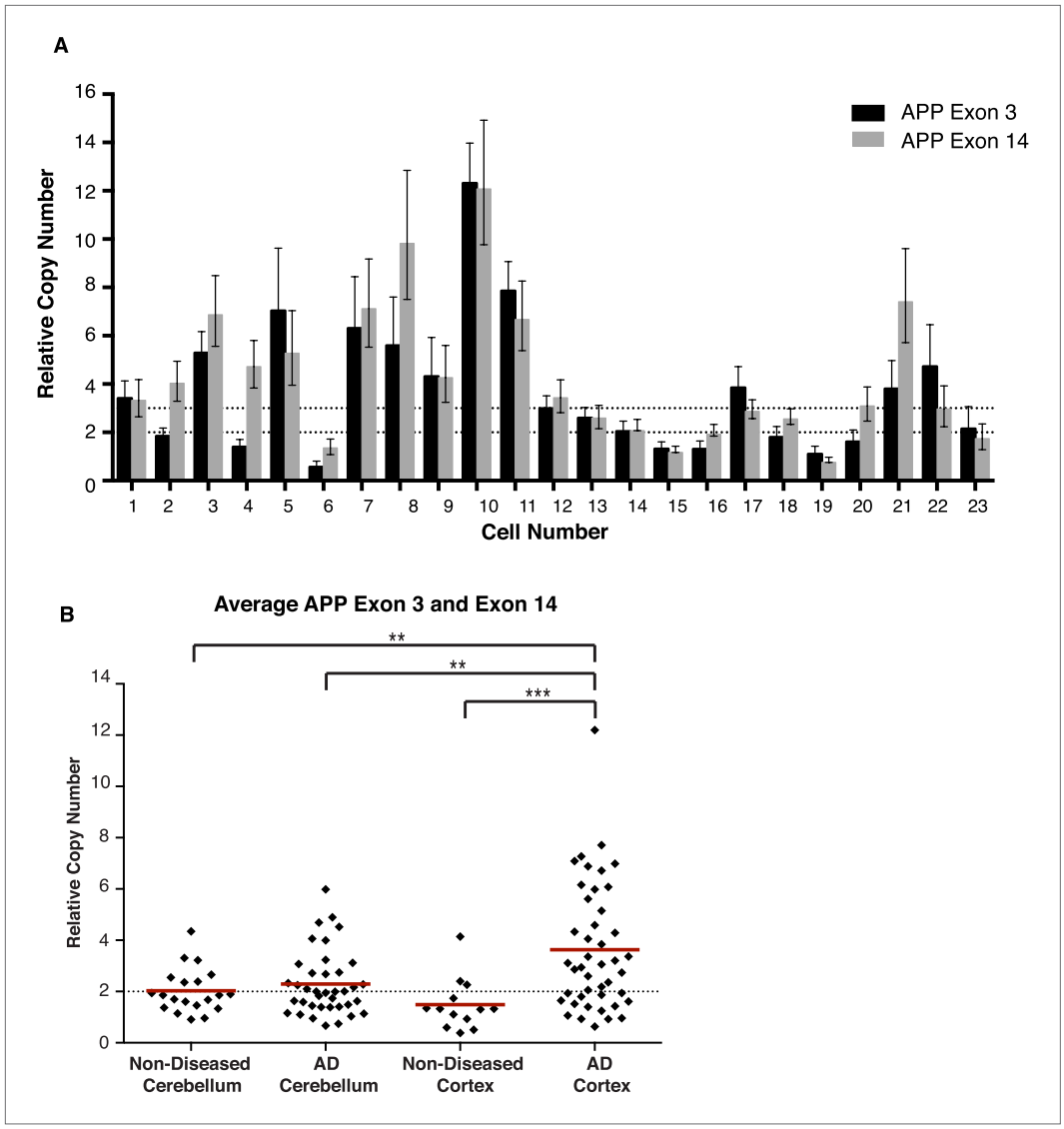

Figure 6—figure supplement 1. Concordance of *APP* exon 3 and 14 from single cell qPCR. (**A**) Relative copy numbers (RCN) for *APP* exon 3 and *APP* exon 14 displaying concordance between exons. 100 of 115 nuclei examined for both exons display copy numbers within one copy number call. 10 of the 15 remaining nuclei, while more than one copy number apart, were both called as gains. Bars represent RCN Min and RCN Max. (**B**) Scatter plot of average relative copy numbers. The data remain consistent with those displayed for individual exons (***Figure 6A,B***). Statistics represent an ANOVA with a Tukey's multiple comparison test. **p < 0.01, ***p < 0.001.

DOI: 10.7554/eLife.05116.015

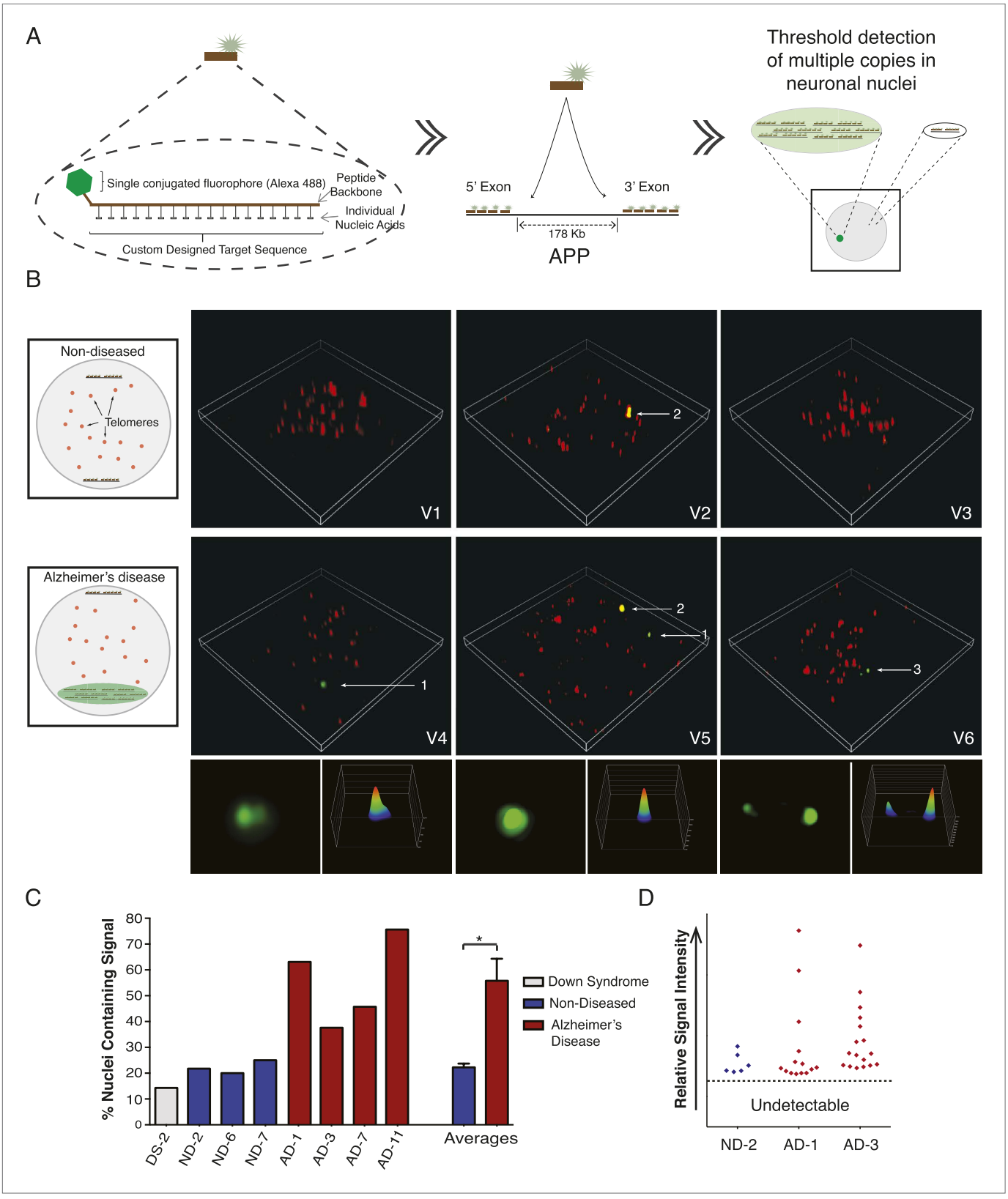

Figure 7. Visualization of *APP* copy number increases in neuronal nuclei from AD brain samples. (**A**) Peptide nucleic acid probes (PNA) were developed against nine separate sites on *APP* (4 sites within exon 3 and 5 sites within exon 14). Each PNA probe consists of a peptide backbone conjugated to a

Figure 7. Continued on next page

Figure 7. Continued

single fluorophore, with separately conjugated nucleotides, substantially increasing specificity (***Lansdorp et al., 1996***). Single copies of *APP* are not detectable because of fluorophore detection limits. Detection of increased copy number by PNA probes can be visualized as copies of *APP* increase (***Figure 7—figure supplement 1B,C***). Positive internal controls using PNA probes directed against telomere sequences were simultaneously hybridized. (**B**) Visualization of copy number increases in neuronal nuclei. Green puncta (arrow 1, insets) indicate visualized *APP* increases. Telomere labeling (red puncta) was present in all nuclei, demonstrating probe accessibility and template fidelity. Lipofuscin (arrow 2, orange puncta) was detected in nuclei, visualized by extensive fluorescence signal in all channels, but was eliminated from quantifications. Limited nuclei displayed two green puncta (arrow 3). V1-6 Refers to the supplemental videos where 3-D projections can be visualized. (**C**) Graphic representation of non-diseased (blue) and DS (grey) brains displayed limited numbers of threshold-detected increases in *APP* (***Figure 7—source data 1***). AD (red) brains displayed significant and consistent threshold-detected increases in *APP*. (**D**) Individual threshold-detected *APP* increases were quantified and plotted on a relative intensity scale (blue diamonds: non-diseased, red diamonds: AD). Dotted line represents the threshold below which *APP* copy number was undetectable, only limited puncta were identified in non-diseased nuclei. Bars indicate ± SEM, *$p < 0.05$.

DOI: 10.7554/eLife.05116.016

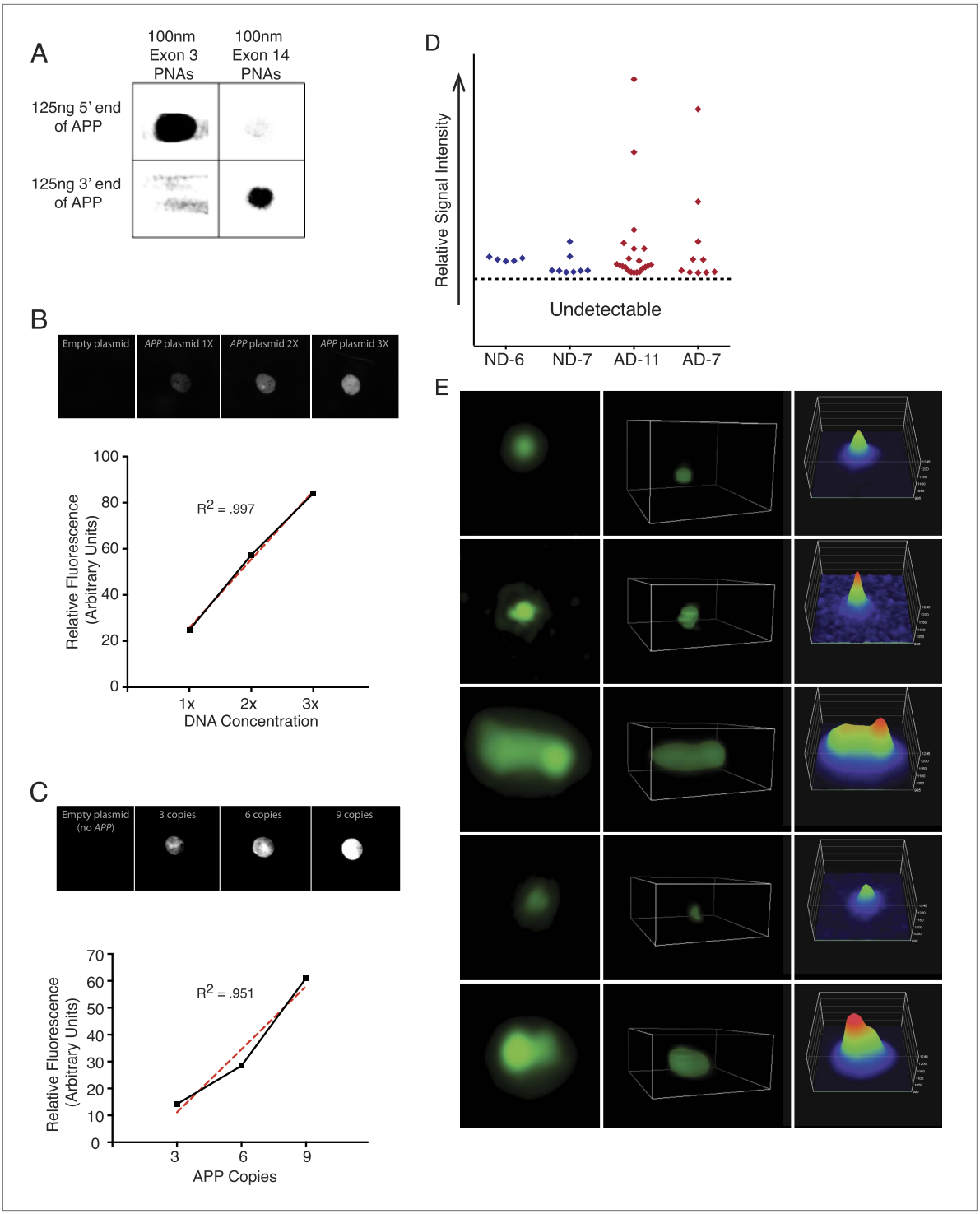

Figure 7—figure supplement 1. PNA FISH controls. (**A**) *PNA* probe specificity was verified via dot blots of *APP* sequence followed by PNA probe hybridization and immunoblotting against the Alexa-488 fluorophor. Probes designed against exon 3 exhibited specific binding to the 5′ region of *APP*, and probes designed against exon 14 exhibited specific binding to the 3′ region of *APP*, while probes did not display significant binding to non-specific sequences. (**B**) Plasmids containing all 9 *APP* PNA binding sites were blotted at 1× (1.8 μg), 2× (3.6 μg), and 3× (5.4 μg) DNA concentration, and PNA probes were hybridized and an empty plasmid at 1.8 μg was used for a negative control in lane 1. Fluorescent output demonstrated a linear increase with increasing DNA concentration. (**C**) 10 μg of plasmids containing 0, 3, 6, and 9 copies of the *APP* PNA binding sites was blotted onto membrane and probes were hybridized. Fluorescent output showed an expected linear increase with the number of PNA probe binding sites. (**D**) Quantification of the variable *APP* signal increases observed across four brains. (**E**) Representative *APP* signals visualized and verified using super-resolution 3D projections displayed a range of variable intensities.

DOI: 10.7554/eLife.05116.018